RSC Advances

PAPER

View Article Online
View Journal | View Issue

Cite this: *RSC Adv.*, 2014, **4**, 16153

Analytical prediction of liquid-gated graphene nanoscroll biosensor performance†

Hediyeh Karimi,[ab] Mohammad Taghi Ahmadi,[cd] Elham Khosrowabadi,[e] Rasoul Rahmani,[a] Mehdi Saeidimanesh,[d] Razali Ismail,*[c] Seyed Danial Naghib[f] and Elnaz Akbari[a]

The latest discovery of the graphene nanoscroll has provided enormous new stimuli to carbon nanoresearch. Due to its one-dimensional structure and tunable core size, the graphene nanoscroll is suitable for nanoscale applications such as in nanotransistors, and biosensor devices. DNA sensing is critical in the identification of the genetic risk factors associated with complex human diseases, and continues to have an emerging role in therapeutics and personalized medicine. This paper presents the analytical model of liquid-gated field effect transistors (LGFETs) for zig-zag graphene nanoscrolls (ZGNSs) inspired by carbon nanotube behavior when exposed to DNA molecules. First of all, in order to gain physical insight into GNS-based devices, the conductance of GNSs is analytically modelled. Based on the sensing mechanism of the DNA sensor, GNS controlling elements (η_{GNS} and ε_{GNS}) are proposed and the behavior of LGFETs-based GNS nanomaterial in the presence of DNA molecules is predicted to get a greater insight into the rapid development of DNA sensors and their application. Because of the channel-doping effect due to the adsorption of the DNA molecules, the conductance of the channel is altered. On the other hand, the applied voltage effect in the form of tilted electron energy levels is utilized in the form of normalized Fermi energy variation which is used in the sensor modelling. This study emphasizes the promising nature of carbon nanoscrolls for a number of electronic device applications.

Received 9th December 2013
Accepted 13th February 2014

DOI: 10.1039/c3ra47432a

www.rsc.org/advances

1. Introduction

Nanosized materials have attracted the attention of scientists due to their wide range of applications in nanoelectronics, medical diagnostics and drug delivery, as a result of their large surface-to-volume ratio, small size and chemical reactivity.[1,2] Despite its short history since its discovery, graphene, which is formed when graphite is broken down into layers, possess extraordinary properties. Two-dimensional graphene is the basic structural element of some carbon allotropes including graphite, single wall carbon nanotubes (SWCNTs), and graphene nanoscrolls (GNSs), as seen in Fig. 1. The SWCNTs can be considered as a cylindrical roll-up of the planar graphene sheet with a sp^2 bonding of carbon atoms.

In recent years, an increasing amount of literature on carbon-based materials has demonstrated that they have great potential applications in nanoelectronics, biosensing, and energy storage owing to their ballistic transport,[3] biocompatibility and stability.[4–6] Among these allotropes, one-dimensional conductors such as SWCNTs and GNSs can act as high-gain liquid-gated field-effect transistors (LGFETs), in which the conductance varies

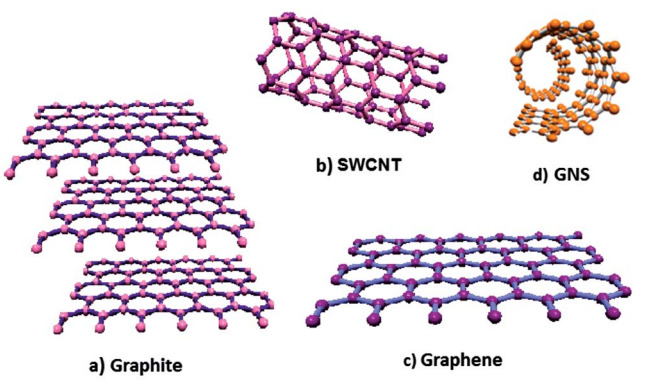

Fig. 1 Carbon-based structures including: (a) graphite, (b) SWCNT, (c) graphene, (d) GNS.

[a]*Centre for Artificial Intelligence and Robotics, Universiti Teknologi Malaysia, 54100 Kuala Lumpur, Malaysia*

[b]*Malaysia Japan International Ins. of Technology, Universiti Teknologi Malaysia, 54100 Kuala Lumpur, Malaysia*

[c]*Computational Nanoelectronic Research Group, Faculty of Electrical Engineering, Universiti, Teknologi Malaysia, 81310, Johor, Malaysia. E-mail: razali@fke.utm.my*

[d]*Nanotechnology Research Center Nanoelectronic Group, Physics Department, Urmia University, 57147, Urmia, Iran*

[e]*Department of Biotechnology and Medical Engineering, Faculty of Biosciences and Medical Engineering, Universiti Teknologi Malaysia, 81310, Johor, Malaysia*

[f]*Department of Chemical Engineering and Materials, University of Calabria, Via P. Bucci, 87036 Rende (CS), Italy*

† Electronic supplementary information (ESI) available. See DOI: 10.1039/c3ra47432a

strongly with the local charge density.[7] According to their carbon-based structure and properties, SWCNTs have been demonstrated as a powerful tool to satisfy our major requirement of a biosensing material for the detection of various biomolecules such as protein, DNA, *etc*.[8–11,12] The development of personalized medicine in which medical treatment is customized to an individual on the basis of genetic information requires techniques that can detect DNA quickly and cheaply.[13,14] The above-mentioned materials have shown extreme sensitivity towards environmental perturbations such as electronic doping[15–18] and molecule adsorption.[12,19–22] Consequently, carbon-based materials are selected as a sensing template for DNA detection in this study. By the molecular analysis of nucleic acids, nearly 400 genetic diseases are diagnosable and this number is rising daily[23] which makes DNA detection urgent for investigation.[24] The growing need for cheaper and faster DNA sensing has prompted the development of new technologies that surpass conventional methods and materials in terms of speed and cost.[25,26]

An attention-grabbing nanomaterial, GNSs, has emerged as a new carbon-based structure which is made by rolling a graphene layer to form an open cylindrical structure.[27] They are predicted to exhibit some exciting electronic and mechanical properties due to their novel structure.[27–30] The electrical properties of GNSs are moderately insensitive to exterior factors because of their self-encapsulated structure where the electrical performance of SWCNTs varies with the primary substrate and the environment.[31] What makes the GNSs more amenable to intercalation or doping is due to the fact that their interplanar distance can be easily changed because GNSs are open at both ends, contrasting with SWCNTs which are wound into closed cylinders. As depicted in Fig. 2, the chirality of the GNS is defined as $\vec{C} = n\vec{a_1} + m\vec{a_2}$ where the nomenclature can be described as zig-zag for $\varphi = 0$, armchair for $\varphi = 90$, and chiral for $0 < \varphi < 90$.[32] The Archimedean-type spiral of GNSs is drawn in Fig. 2, where N_{turn} is the number of turns, r_{in} is the inner radius and $d_{int} \approx 0.34$ Å is the interlayer distance that is experimentally obtained.[12]

As the graphene sheet is theoretically rolled into a (one-dimensional) 1D cylindrical tube, a gap will form at the Fermi point; and, therefore, convert its properties from metallic to semiconducting. Unlike SWCNTs, GNS properties cannot be determined comprehensively by its chirality (n,m)[27] owing to the fact that its core size alters its properties. This characteristic indicates dependency of GNS properties on its geometry.[29,30] It is notable that the GNS interlayer is capable of holding more dopants because its diameter can be expanded to contain the volume of the dopant–layer interactions.[33–36] GNSs are affected by the interlayer interaction between the inner and outer layers compared to SWCNTs; thereby, GNSs are expected to exhibit a higher on-current than SWCNTs for the same diameter. Most researchers to date have tended only to focus on molecular dynamics and simulations to reveal the configuration and stability of the GNSs.[32,36,37] However, Pan *et al.* have discussed the electronic structure and optical properties of GNSs in much details.[38] Surveys such as that conducted by them have shown that two specific structures of nanoscrolls with different properties exist: one is the armchair nanoscroll (AGNS) of the type (n,n), and those of type $(n,0)$ the zig-zag nanoscroll.[27,32] Braga *et al.* have identified that ZGNSs show semiconducting and semi-metallic properties whereas AGNS exhibit metallic properties. The semiconducting property is essential for the implementation of LGFETs, thus, ZGNS is being considered as a new biosensing template in this paper.

2. The proposed structure of DNA sensor-based graphene nanoscroll

The LGFET-based SWCNTs have been successfully fabricated using nano-/micro-lithographic fabrication.[39,40] However, there is still no experimental result that predicts the behavior of GNS-based biosensors as a detector of DNA molecules.[41] The aim of this study is to propose a biosensor-based GNS nanomaterial model and predict its behavior in the presence of DNA molecules, based on SWCNTs, to get a greater insight into the rapid development of DNA sensors and their application. Supporting this idea, the sensing mechanism of SWCNTs-based DNA sensors needs to be understood perfectly. As shown in Fig. 3, the proposed structure of the GNS-based DNA sensor consists of a source and drain, in which the GNSs are employed as a conducting channel on an oxidized Si/SiO_2 substrate. Since the GNS is a 1D tube-like structure and exhibits semiconductor properties, it can be possibly fabricated as a top-gated planar device like an SWCNT-based FET. The top-gated planar device has several advantages over back-gated devices, such as low voltage switching, an enhanced sub-threshold slope (SS) and drain-induced barrier lowering (DIBL). Therefore, the top gates can control the current through the GNS channel. A photoresist layer as an insulator will be employed that results in the

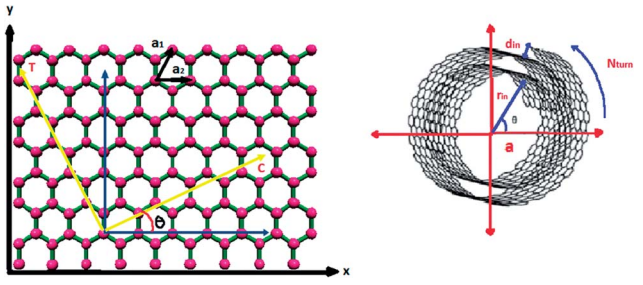

Fig. 2 The unrolled graphene layer as the basic of GNSs, in which φ is the scroll angle with respect to the *xy* axes, *C* and *T* are the scroll vector and translational vector respectively.

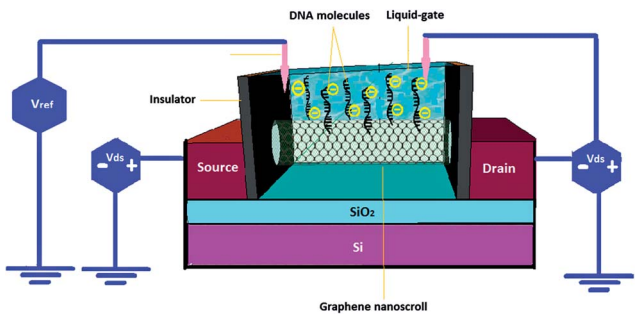

Fig. 3 Proposed structure of LGFET-based new materials of GNSs for DNA detection.

creation of a small window that exposes to the electrolyte containing DNA molecules.[42] The electrical detection of DNA molecules can be measured by recording the conductance of the GNS channel before and after DNA immobilization.[43] Furthermore, the potential of GNS is controlled with respect to a reference electrode.[44] As π-electrons are delocalized on the surfaces of GNSs, their conductance is tremendously influenced by the adsorbed charges of DNA molecules taking place adjacent to the carbon surfaces.[45] The conductivity of the LGFET-based-GNS sensor is altered by the charge carrier density changing in the conducting channel with the presence of DNA molecules.[46,47] In this paper, the effect of the DNA molecule presence in the conductance of the GNS channel is estimated upon on the significant shift of the G–V_g characteristic of LGFET-based DNA sensors.[48,49]

Although numerical simulation does give us more accurate results, they are time consuming for fast circuit simulation compared to analytical ones.[50] Therefore, in order to gain physical insight into GNS-based devices, the conductance of GNSs will be analytically modelled.[51–53]

3. Proposed model

Conductance is considered an essential parameter which plays a critical role in determining the characteristics of LGFETs and electrical properties such as current–voltage characteristics.[50,51] Conductance is chosen as a measurable sensing parameter in this study due to the fact that carbon-based materials are so sensitive to the introduction of DNA molecules. On the other hand, the (π–π) interaction between DNA molecules and the surface of carbon materials results in a change in conductance of the LGFETs.[54,55] It can be a reasonable justification to start the modelling from the conductance of carbon allotropes. In this paper, carbon-based materials analysis as a DNA sensor platform is in our focus; therefore, SWCNTs and GNSs as carbon-based materials that are fundamental building blocks in structural and electrical points of view are extensively investigated. We will start with SWCNTs.

3.1 Conductance modelling of SWCNTs

Modelling of the band structure of SWCNTs began from the energy dispersion relation of the graphite sheet (graphene) band structure. The band energy throughout the entire Brillouin zone of graphene is[56]

$$E(\vec{k}) = \pm t\sqrt{1 + 4\cos\left(\frac{k_x 3a_{C-C}}{2}\right)\cos\left(\frac{k_y\sqrt{3}a_{C-C}}{2}\right) + 4\cos^2\left(\frac{k_y\sqrt{3}a_{C-C}}{2}\right)} \quad (1)$$

where $a_{C-C} = 1.42$ Å is the carbon–carbon (C–C) bond length, $t =$ 2.7 (eV) is the nearest neighbor C–C tight binding overlap energy, and $k_{x,y,z}$ is wave vector component.[57] By using a Taylor series expansion for the cosine function near the Fermi point, the $E(k)$ relation of the SWCNTs is:

$$E(\vec{k}) = \frac{t\,3a_{C-C}}{2}\sqrt{\beta^2 + {k_x}^2} \quad (2)$$

where k_x represents the wave vector along the length of the nanotube, which can be extracted in the parabolic part of the band energy as

$$k_x = \sqrt{\frac{4E}{3a_{C-C}t} - \frac{8}{9d^2}} \quad (3)$$

where d is the diameter of the SWCNT and β is the wave vector component along the circular direction, which is quantized by the periodic boundary condition. Moreover, for the lowest band of SWCNTs, β is at a minimum, and for metallic SWCNTs, the minimum value for β is zero. For semiconducting SWCNTs, the minimum magnitude of the quantized wave vector is $\beta = 2/3d$.[58] By substituting this equation into $E(k)$, an approximation for the semi-conducting SWCNTs is obtained as[59]

$$E(\vec{k}) = \pm\frac{t\,3a_{C-C}}{2}\sqrt{\left(\frac{2}{3d}\right)^2 + {k_x}^2} \quad (4)$$

The (±) signs are related to the valence and conductance bands. When the related energy covers the bottom of the conduction band, the parabolic approximation can be applied on the band diagram holding the fact that the sub-band location has a strong effect on the number of modes. In other words, the mode density $M(E)$ raises with energy.[59] Taking into consideration the spin degeneracy, the number of conductive channels can be calculated as:

$$M(E) = 2\frac{\Delta E}{\Delta k L} = \frac{3a_{C-C}t}{L}\sqrt{\frac{4E}{3a_{C-C}t} - \frac{8}{9d^2}} \quad (5)$$

where the channel length is shown by L. Two issues contribute to the conductance output in large channels which make it capable of following the Ohmic scaling law based on the Landauer formula. The first factor is independent of the length which is the interface resistance. The second is due to the non-linearity relation between the conductance and width which depends upon the number of modes in the conductor. So the conductance from the Landauer formula can be extended in the form of eqn (6) while these quantized parameters are considered:

$$G = \frac{2q^2}{h}\int_0^{+\infty} M(E)T(E)\left(-\frac{\mathrm{d}f(E)}{\mathrm{d}E}\right)\mathrm{d}E \quad (6)$$

where q is the electron charge, h is Planck's constant, and T is the transmission probability. Because of the ballistic transport of graphene, T approximates to one ($T(E) = 1$). Moreover, $f(E)$ is the probability of occupation of the Fermi level with electrons which is known as the Fermi–Dirac distribution function as[61–63]

$$f(E) = \frac{1}{e^{\frac{E-E_F}{k_B T}} + 1} \quad (7)$$

where E_F is the Fermi energy, k_B is the Boltzmann constant and T is the temperature. According to the Maxwell–Boltzmann approximation, the distribution function can be expressed as

$$f(E) \approx \frac{1}{e^{\frac{E-E_F}{k_B T}}} = e^{-\frac{E-E_F}{k_B T}} \quad (8)$$

The length of the SWCNT as a function of conductance plays a significant role in defining the conductivity equation.[64] By replacing the number of sub-bands (mode numbers) incorporated with the Fermi–Dirac distribution function in eqn (3), the conductance can be obtained as

$$G = \frac{2q^2}{h}\frac{3a_{C-C}t}{L}\sqrt{\frac{4}{3a_{C-C}t}}\int_0^{+\infty} M(E)T(E)\left(-\frac{\mathrm{d}f(E)}{\mathrm{d}E}\right)\mathrm{d}E \quad (9)$$

By making the substitution of $x = (E - E_g)/k_BT$, the boundary of integral changes as follows and eqn (9) becomes

$$G = \pm\frac{6q^2}{hL}(a_{C-C}t\pi k_BT)^{1/2}\left(\int_0^{+\infty}\frac{x^{-1/2}}{(1+e^{x-\eta})}\mathrm{d}x + \int_0^{+\infty}\frac{x^{-1/2}}{(1+e^{x+\eta})}\mathrm{d}x\right) \quad (10)$$

where the normalized Fermi energy is defined as $\eta = (E_F - E_g)/k_BT$. Applying the Fermi–Dirac integral form of conductance is useful for understanding the role of degenerate and non-degenerate regimes. It is noted that the Fermi–Dirac integral (FDI) of order i is defined as

$$\Im_i(\eta) = \frac{1}{\Gamma(i+1)}\int_0^{\infty}\frac{x^i}{1+e^{x-\eta}}\mathrm{d}x \quad (11)$$

In general $\Gamma(i+1) = \int_0^{\infty} e^{-x}x^i\mathrm{d}x = i!$ if i is an integer applicable to the gamma function, $\Gamma(1/2) = \pi$ and $\Gamma(3/2) = (1/2)\Gamma(1/2) = \pi/2$. It is significant to observe the general properties of the FDI in the non-degenerate and the strongly degenerate limits. Thus, the general conductance model of the SWCNT can be obtained similar to that of silicon as reported by Gunlycke *et al.*,[67]

$$G = \mp\frac{6q^2}{hL}(a_{C-C}t\pi k_BT)^{1/2}\left(\Im_{-1/2}(\eta) + \Im_{-1/2}(-\eta)\right) \quad (12)$$

where $\Im_{-1/2}(\eta)$ is the Fermi–Dirac integral of order $(-1/2)$. The Fermi–Dirac distribution function has attributed to degenerate and non-degenerate states with the amount of $(\eta \gg 0)$ and $(\eta \ll 0)$ respectively.[65,66] In the degenerate state, on the other hand, the concentration of electrons in the conduction band exceeds the density of states and the Fermi energy lies within the conductance band and the Fermi–Dirac function can be approximated as $\eta(E) = 1$. The non-degenerate limit occurs when the 1 is neglected from the denominator. In the non-degenerate state there are few electrons in the conduction band and the edge of the conduction band is far above the Fermi energy compared to k_BT. In this limit, in spite of the value of the normalized Fermi energy, the Fermi–Dirac integral can be approximated by the Maxwell–Boltzmann distribution factor of $\eta(E) = \exp(\eta\cdot\eta)$. Thus, in the non-degenerate limit, the general conductance model of the SWCNT can be converted into the exponential equation as

$$G = \mp\frac{6q^2}{hL}(a_{C-C}t\pi k_BT)^{1/2}\left(e^{(\eta)} + e^{(-\eta)}\right) \quad (13)$$

As the normalized Fermi energy is derived as $\eta = (E - E_g)/k_BT$, and the band gap energy is $E_g = qv_g$, then the normalized Fermi energy is obtained as $\eta = (V_t - V_g)/k_BTq$, which represents a function of V_g. Employing η in eqn (13), the conductance can be expressed as

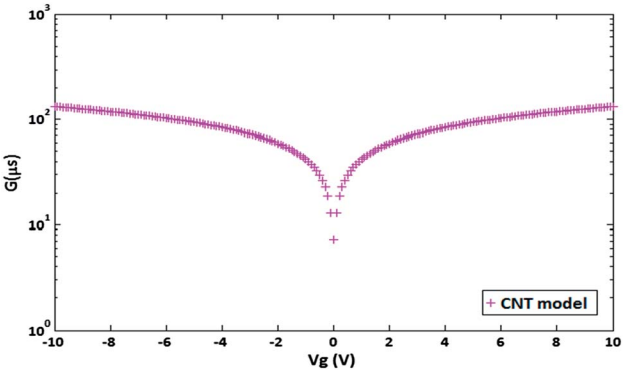

Fig. 4 Conductance model of SWCNT-based LGFETs without the presence of DNA molecules.

$$G = \mp\frac{6q^2}{hL}(a_{C-C}t\pi k_BT)^{1/2}\left(e^{(V_t-V_g)/k_BTq)} + e^{(-V_t+V_g)/k_BTq)}\right) \quad (14)$$

which represents the conductance (G) as a function of the gate voltage (V_g). Fig. 4 illustrates the SWCNT-based DNA sensor conductance model *versus* the gate voltage for a non-degenerate regime before adding any DNA molecule. According to the experimental data, the proposed model can satisfy our major requirement of a carbon nanotube-based DNA sensor.[47]

In this work, the conductance model of the SWCNT as a sensing parameter is employed in the DNA sensor modelling, also to give us an extensive chance of explaining the device characteristics.

3.2 Conductance model of the GNS

In this part, in order to understand the electrical properties of GNSs and describe their physical phenomena, the energy band for 1D GNSs is modelled. The electrical properties of the GNS can be differentiated by the structure and exhibited through the energy spectrum. What we know about GNS carrier statistics is largely based upon theoretical studies that compute its energy spectrum and the behavior of the band gap in terms of the chirality factor.[15] Surveys such as that conducted by Braga *et al.* have shown that the ZGNSs exhibit semiconducting and semimetallic properties.[16] The semiconducting property is essential in MOSFET implementation, thus, the ZGNS is being considered in this paper. Eqn (15) shows the tight binding model for the ZGNS energy spectrum throughout the Brillouin zone of the GNS[15,17]

$$E_{ZGNS}(k) = \pm t\sqrt{1 + 4\cos\left(\frac{3k_xa_{C-C}}{2}\right)\cos\left(\frac{2\pi\nu - \varphi}{2n}\right) + 4\cos^2\left(\frac{2\pi\nu - \varphi}{2n}\right)} \quad (15)$$

where k_x is the wave vector along the x-axis, a_{C-C} represents the length of the carbon–carbon bond and the chirality of the ZGNS (n,m) is shown by n. Moreover, φ is the scroll angle with respect to the xy-axes which is the only parameter that can control the geometry of the GNS as well as the energy gap.[1] The chirality has a strong influence on the band structure of the GNS, so the considered boundary condition of $\vec{k}\,\vec{C} = 2\pi\nu - \varphi$, where

$v = 1,2, \ldots, 2n$ is defined as the number of sub-bands for a particular $(n,0)$ chirality. Here, $\vec{C}$ is the scroll vector as outlined schematically in Fig. 2 and $\vec{k}$ denotes the wave vector. The shape of the GNS is at equilibrium at the φ parameter and it is used to quantize the k-vectors in a different manner.[18] Chen *et al.* discussed the electronic structure dependence of the fundamental parameters of the GNS *via* a first-principals calculation based on density functional theory (DFT) and the local density approximation (LDA) in 2007.[18] It is noteworthy to point out that just the first unfilled energy level (conduction band) at $T = 0$ K is being considered, holding the fact that the possibility of occupying this level by electrons is high. Eqn (15) gives the expression for the $E(K)$ relation throughout the Brillouin zone of the GNS. But the main interest is the band structure near the Fermi point in the Brillouin zone of the GNS. Then, by employing a Taylor series expansion, eqn (15) is approximated to be

$$E_{\mathrm{ZGNS}} = \pm 3t\sqrt{1 + \frac{5}{8}k_x{}^2 a_{\mathrm{C-C}}{}^2} \tag{16}$$

The positive sign denotes the conduction band and the negative sign the valence band. In order to obtain the conductance based on the Landauer formula, the number of sub-bands in the GNS channel must be considered. In other words, the mode density $M(E)$ increases with energy.[59] The number of conducting channels in the GNS is defined as

$$M(E) = \frac{\Delta E}{L\Delta K} = \mp\frac{9a^2 t}{4L}\sqrt{\frac{8E}{9ta^2} \pm \frac{4}{9a^2}} \tag{17}$$

In the conductance of nanoscale materials like GNS, two quantizing parameters play a dominant role: these are the number of sub-bands, and interface resistance, both which are independent of the length.[60]

A region of minimum conductance *versus* the gate voltage is calculated by $G_0 = 2q^2/h$. So, the conductance model of the GNS channel can be assumed as:

$$G = \mp\frac{9q^2 a_{\mathrm{C-C}}{}^2 t}{2hLk_{\mathrm{B}}T}\int_0^{+\infty}\left(\frac{\left(\frac{8E}{9ta_{\mathrm{C-C}}{}^2} \pm \frac{4}{9a_{\mathrm{C-C}}{}^2}\right)^{1/2} e^{\frac{E-E_F}{k_{\mathrm{B}}T}}}{\left(1 + e^{\frac{E-E_F}{k_{\mathrm{B}}T}}\right)^2}\mathrm{d}E\right) \tag{18}$$

In order to obtain a simplified form of conductance, the partial integration method is used where $x = (E - E_g)/k_{\mathrm{B}}T$ and the normalized Fermi energy is $\eta = (E - E_g)/k_{\mathrm{B}}T$. Finally, the general conductance model of the GNS obtained:

$$G = \mp\frac{9q^2 a_{\mathrm{C-C}}{}^2 t}{2hL}\int_0^{+\infty}\left(\frac{\left(x + \frac{E_g}{k_{\mathrm{B}}T} \pm \frac{t}{2k_{\mathrm{B}}T}\right)^{1/2}\left(\frac{8}{9a_{\mathrm{C-C}}{}^2 t}\right)^{1/2}(e^{x-\eta})}{(1 + e^{x-\eta})^2}\right)\mathrm{d}E \tag{19}$$

The analytical model of GNS conductance is plotted in Fig. 5.

Conductance *versus* the gate voltage of the GNS is obtained in this section which is expected to help us to gain a broader insight into GNS-based LGFETs compared with SWCNTs.

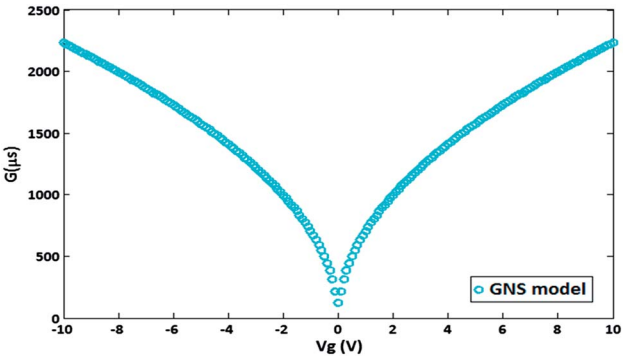

Fig. 5 Conductance model of GNS-based LGFETs without the presence of DNA molecules.

3.3 Results and discussion

In order to understand the physical structure and electronic properties of GNSs in DNA sensor applications, the conductance model of SWCNTs and the distinct features between both structures that influenced their electronic properties are discussed here. As depicted in Fig. 6, the conductance of SWCNTs and GNSs is illustrated in the form of related LGFET structures. By applying the gate voltage between −10 and 8 V, a bipolar characteristic of the LGFET device is observed in view of the fact that the Fermi energy can be controlled by the gate voltage. Because of this characteristic, these materials have the potential to be switched from the p-doped to the n-doped region by changing the gate voltage continually. As outlined in ref. 20, the minimum conductance (g_{min}) at the switch point where the density of electron and hole carriers is equal can be used to monitor the doping state of the SWCNT/GNS. This switch point also is known as the charge-neutrality point (CNP). It has been demonstrated that different n-dopant biomolecules can affect the conductance of the LGFET device. As depicted in Fig. 6, by immobilization of the DNA molecule as an n-dopants on the carbon nanotube surface, the conductance is dramatically decreased. As a result, it can be concluded that the conductance of the SWCNT/GNS channel would be very sensitive to the immobilization of DNA. To evaluate the presented model we need to compare it with experimental work,[24] which is not available for GNSs. Therefore, in order to predict the GNS

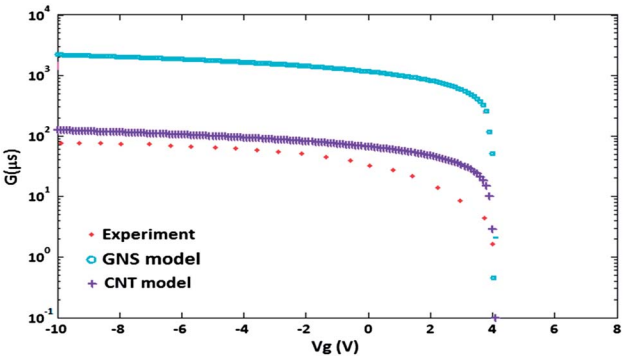

Fig. 6 Conductance model of SWCNT-based LGFETs without the presence of DNA molecules.

behavior in the presence of DNA molecules, the proposed model of the DNA sensor-based SWCNTs is carried out and compared with extracted experimental data for validation.[24] In the second step, the model of the DNA sensor-based GNS will be suggested. In light of this fact, the focus of this paper is to present a new model for GNS-based DNA sensor materials inspired by SWCNTs to predict the capability of DNA detection.

In SWCNT-FET modelling, the DNA concentration as a function of the gate voltage is assumed.[11] Subsequently, the gate voltage is modelled by the DNA concentration as:

$$V_{\mathrm{gs(DNA)}} = \beta V_{\mathrm{gs(without\ DNA)}} \tag{20}$$

where the DNA sensitivity factor (β) is proposed and F is the DNA concentration which can represent the different concentrations of DNA molecules (nM). In the non-saturation area, the DNA sensitivity factor model is utilized as

$$G = \mp\frac{6q^2}{hL}(a_{\mathrm{C-C}}t\pi k_{\mathrm{B}}T)^{1/2}\left(\Im_{-1/2}\left(\frac{(\beta V_{\mathrm{gs(without\ DNA)}} - Vt)q}{k_{\mathrm{B}}T}\right) + \Im_{-1/2}\left(-\frac{(\beta V_{\mathrm{gs(without\ DNA)}} - Vt)q}{k_{\mathrm{B}}T}\right)\right) \tag{21}$$

Thus the DNA sensitivity factor on the SWCNT surface by particle swarm optimization (PSO) is modelled as:

$$\beta = b^{a\mathrm{F}} \tag{22}$$

By the PSO method, the best values for the parameters a, b are obtained as (4720, 1.85) respectively. Moreover, according to the experimental results,[47] increasing the number of DNA molecules has a strong influence on the threshold voltage. Supporting this fact, by increasing the number of DNA molecules, the threshold voltage was also amplified. The carrier concentration has an inverse relation to the DNA concentration therefore the threshold voltage variation can be modelled as $V_{\mathrm{t(with\ DNA)}} = \gamma V_{\mathrm{t(without\ DNA)}}$ where γ is the voltage-controlling factor. Now, the general conductance model of an SWCNT-based DNA sensor in the presence of a normalized Fermi energy $\eta = \frac{(\beta V_{\mathrm{gs(without\ DNA)}} - \gamma V_{\mathrm{t(without\ DNA)}})q}{k_{\mathrm{B}}T}$ is given by

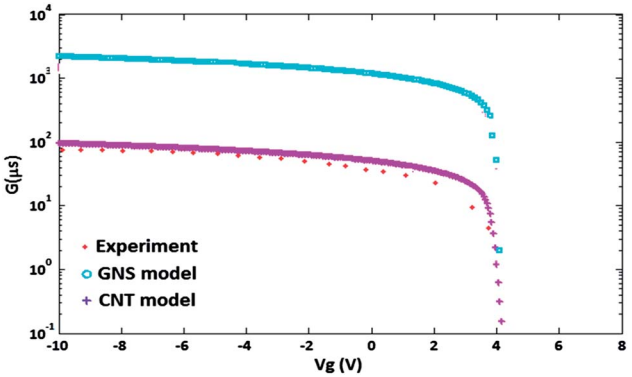

Fig. 7 G–V_{g} characteristics of the proposed β,γ model with the experimental data for SWCNT-based DNA sensors.

It is apparently shown in Fig. 7 that by applying the control factors (β,γ) to the conductance model of the SWCNT, the suggested model is closer to the experimental data; in the same manner, GNS which is immobilized with the DNA molecules can be predicted as well.

Now we are going to predict the behavior of a specific GNS that can be replace the carbon nanotube in DNA-sensor applications. The conductance of the LGFETs-based GNS/SWCNT channel is not only dependent on the sensor structure and operation voltage of the source-drain channel, but also dependent on the physical parameters such as diameter, length, radius and geometry of the GNS and SWCNT channel. The result of this comparison between the SWCNT and GNS conductance models indicates that the GNS shows a superior conductance, $>10G_0$, over the carbon nanotubes.[41] The finding of this current study is consistent with that of Schaper *et al.* reported in 2011.[41] The structural parameters of the GNS are somewhat different from the SWCNT, but the things that remain the same are the certain factors in affecting their electronic properties. Each of these materials has its own structural parameter that influences the electrical properties, though some of the GNS behavior can be related to the SWCNT by its diameter. The electronic properties of SWCNTs are very much influenced by the size of their diameter. However, the electronic properties of GNSs are related to the number of overlapping

$$G = \mp\frac{6q^2}{hL}(a_{\mathrm{C-C}}t\pi k_{\mathrm{B}}T)^{1/2}\left(\Im_{-1/2}\left(\frac{(\beta V_{\mathrm{gs(without\ DNA)}} - \gamma V_{\mathrm{t(without\ DNA)}})q}{k_{\mathrm{B}}T}\right) + \Im_{-1/2}\left(-\frac{(\beta V_{\mathrm{gs(without\ DNA)}} - \gamma V_{\mathrm{t(withoutDNA)}})q}{k_{\mathrm{B}}T}\right)\right) \tag{23}$$

By substituting $\beta = 1.85^{(4720)F}$ and $\gamma = 4.014V_{\mathrm{t}}^{(-1.399)}$ in eqn (23), the conductance model of the SWCNT-based DNA sensor is given by

layers, which can be referred to as N_{turn}. In addition, the inner radius can also affect the properties through varying the diameter size for a constant interlayer distance. Thus, it is fair to

$$G = \mp\frac{6q^2}{hL}(a_{\mathrm{C-C}}t\pi k_{\mathrm{B}}T)^{1/2}\left(\begin{array}{l}\Im_{-1/2}\left(\frac{(1.85^{(4720)F}V_{\mathrm{gs(without\ DNA)}} - 4.014V_{\mathrm{t}}^{(-1.399)}V_{\mathrm{t(without\ DNA)}})q}{k_{\mathrm{B}}T}\right)\\ +\Im_{-1/2}\left(-\frac{(1.85^{(4720)F}V_{\mathrm{gs(without\ DNA)}} - 4.014V_{\mathrm{t}}^{(-1.399)}V_{\mathrm{t(without\ DNA)}})q}{k_{\mathrm{B}}T}\right)\end{array}\right) \tag{24}$$

state that the size of the GNS diameter contributes in controlling the electronic properties.[41] Furthermore, the GNS conductance was investigated through the dependence of its length and diameter as the current density was raised whilst decreasing the length and increasing the diameter.[41] The most interesting advantage of the GNS is its tuneable core size for intercalation with donors and acceptors, and its diameter can be expanded to accommodate the doping volumes, unlike the SWCNT.[36] Because of the GNS tuneable inner radius, research on its electronic and optical capabilities have been reported.[28,30,33,34,68] The results of applied voltage over the semiconducting sample can be seen in the form of tilted electron energy levels which lead to electron movement into the lower energy levels. Therefore the normalized Fermi energy as a function of applied voltage is estimated to change as $\eta_{GNS} = (V_g \times N_{turn} \times (m + n) \times d_{in})/L_{GNS}$. One unanticipated finding is that the GNS behavior depends strongly on the geometrical conditions in such a way that large tube diameters strongly favour the conductance increase, as do shorter tube lengths.[42,69–73] So the proposed conductance of the GNS is modified as:

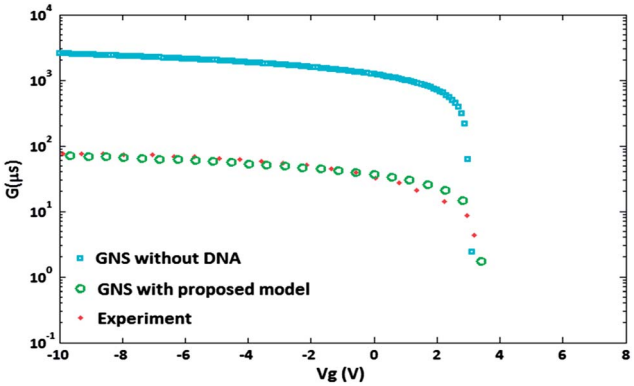

Fig. 8 G–V_g characteristic of proposed the GNS Alpha and Beta model with experimental data for GNS-based DNA sensors.

$$G_{(\text{without DNA})} = \mp\frac{9q^2 a_{C-C}{}^2 t}{2hL}\int_0^{+\infty}\left(\frac{\left(x+\frac{E_g}{k_B T}\pm\frac{t}{2k_B T}\right)^{1/2}\left(\frac{8}{9a_{C-C}{}^2 t}\right)^{1/2}\left(e^{x-\left(V_g\times N_{turn}\times(m+n)\times d_{in}\right)/L_{GNS}}\right)}{\left(1+e^{x-\left(V_g\times N_{turn}\times(m+n)\times d_{in}\right)/L_{GNS}}\right)^2}dE\right) \quad (25)$$

The GNS with these specific characteristics of $N_{turn} = 1.4$, $d_{in} = 0.0396$, $(m,n) = (16,0)$ and $L_{GNS} = 100$ nm is suggested to replace the SWCNT in the DNA sensor platform. The smallest inner diameter for the ZGNS is ~5 Å.[37] The GNS becomes unstable if r_{in} is less than its optimized value due to the greater elastic bending energy than for the van der Waals (VDW) interaction. It is predicted that the conductivity of the GNS-LGFET device is influenced by the charge carrier density changing in the channel by the introduction of DNA molecules to the chamber filled with electrolyte solution.[74] When the GNS is coated with the negative charges of DNA molecules, it is noteworthy that the DNA molecules n-dope the GNS channel. As the number of DNA molecules increases, the conductance of the GNS would be decreased. This fact indicates that by injection of negative charges of DNA molecules to the GNS channel, the number of majority carriers which were holes start to be reduced. And based on what has been discussed, GNS controlling elements are proposed. Therefore, the conductance of the GNS channel in the presence of DNA molecules is predicted as

$$G_{\text{with DNA}} = G_{\text{without DNA}} - \left(\left(\eta_{GNS}\times\frac{G_{\text{without DNA}}}{F}\right) + \left(\varepsilon_{GNS}\times G_{\text{without DNA}}\times V_{tGNS}\right)\right) \quad (26)$$

where $G_{\text{with DNA}}$ and $G_{\text{without DNA}}$ are the channel conductance of the GNS with and without DNA molecules respectively, η_{GNS} and ε_{GNS} are the GNS controlling elements, V_{tGNS} can vary between 0.2 and 1, and $F = 5000$ nM. Consequently, the supposed conductance model of the LGFET-based GNS channel can be obtained by replacing eqn (25) and $\eta_{GNS} = (V_g \times N_{turn} \times (m + n) \times d_{in})/L_{GNS}$ in eqn (26). By employing the PSO method, the parameters are obtained as $\eta_{GNS} = 800$, $\varepsilon_{GNS} = 12$. In Fig. 8, when the device is exposed to the solution of DNA, the model is closer to the experimental result and the conductance of the GNS will be reduced by about 1400 μs; in the same way we can evaluate other experimental data. It is actually shown that by altering DNA concentration through the GNS controlling elements,the G–V_g characteristic curve can be managed.

4. Conclusion

The emergence of GNSs that offer more flexibility in terms of adjustable band energy and providing a large detection area could contribute to facilitating device scaling and fabrication. The high conductivity and current density values of GNSs as well as their switching capabilities make the GNS-type nanotubes strong candidates in sensor technology. In this work, the SWCNT analytical model of biosensors is included in the derivation of a GNS-based DNA sensor model to understand the geometry effects on the sensing parameters. Furthermore, the possibility of DNA molecule detection by presenting the analytical model of liquid-gated transistor (LGFETs) for zig-zag graphene nanoscrolls (ZGNSs) inspired by carbon nanotubes is addressed. Developing GNS-based biosensors becomes practical by understanding the sensing mechanism. Therefore, the conductance of the GNS as a sensing parameter is analytically investigated. Moreover, the applied voltage effect in the form of tilted electron energy levels is used to vary the normalized Fermi energy. Also, channel doping due to the GNS–nucleotide interaction effect on the conductance of the LGFET device is considered. To model this behavior, the GNS controlling elements (η_{GNS} and ε_{GNS}) are proposed and behavior of the LGFET-based GNS nanomaterial in the presence of DNA molecules is estimated, and the proposed model is simulated in same manner as for SWCNTs.

Acknowledgements

The authors would like to acknowledge the financial support from Research University grant of the Ministry of Higher Education (MOHE), Malaysia under project number Q.J130000.2523.04H99. Also thanks to the Research Management Centre (RMC) of Universiti Teknologi Malaysia (UTM) for providing excellent research environment in which to complete this work.

References

1 A. J. Mieszawska, R. Jalilian, G. U. Sumanasekera and F. P. Zamborini, The Synthesis and Fabrication of One-Dimensional Nanoscale Heterojunctions, *Small*, 2007, **3**, 722–756.

2 L. Chu, Q. Xue, T. Zhang and C. Ling, Fabrication of Carbon Nanoscrolls from Monolayer Graphene Controlled by P-Doped Silicon Nanowires: A MD Simulation Study, *J. Phys. Chem. C*, 2011, **115**, 15217–15224.

3 J. H. Warner, M. H. Rümmeli, L. Ge, T. Gemming, B. Montanari, N. M. Harrison, *et al.*, Structural transformations in graphene studied with high spatial and temporal resolution, *Nat. Nanotechnol.*, 2009, **4**, 500–504.

4 K. S. Novoselov, A. K. Geim, S. V. Morozov, D. Jiang, Y. Zhang, S. V. Dubonos, *et al.*, Electric Field Effect in Atomically Thin Carbon Films, *Science*, 2004, **306**, 666–669.

5 K. S. Novoselov, D. Jiang, F. Schedin, T. J. Booth, V. V. Khotkevich, S. V. Morozov, *et al.*, Two-dimensional atomic crystals, *Proc. Natl. Acad. Sci. U. S. A.*, 2005, **102**, 10451–10453.

6 X. Dong, X. Zhao, L. Wang and W. Huang, Synthesis and Application of Graphene Nanoribbons, *Curr. Phys. Chem.*, 2013, **3**, 291–301.

7 S. Sorgenfrei, C.-y. Chiu, R. L. Gonzalez Jr, Y.-J. Yu, P. Kim, C. Nuckolls, *et al.*, Label-free single-molecule detection of DNA-hybridization kinetics with a carbon nanotube field-effect transistor, *Nat. Nanotechnol.*, 2011, **6**, 126–132.

8 F. Schedin, A. K. Geim, S. V. Morozov, E. W. Hill, P. Blake, M. I. Katsnelson, *et al.*, Detection of individual gas molecules adsorbed on graphene, *Nat. Mater.*, 2007, **6**, 652–655.

9 K. Welsher, Z. Liu, D. Daranciang and H. Dai, Selective Probing and Imaging of Cells with Single Walled Carbon Nanotubes as Near-Infrared Fluorescent Molecules, *Nano Lett.*, 2008, **8**, 586–590.

10 M. Wu, R. Kempaiah, P.-J. J. Huang, V. Maheshwari and J. Liu, Adsorption and Desorption of DNA on Graphene Oxide Studied by Fluorescently Labeled Oligonucleotides, *Langmuir*, 2011, **27**, 2731–2738.

11 F. Karimi, M. Ahmadi, M. Rahmani, E. Akbari, M. J. Kiani and M. Khalid, Analytical Modeling of Graphene-Based DNA Sensor, *Sci. Adv. Mater.*, 2012, **4**, 1142–1147.

12 Y. Shi, X. Dong, P. Chen, J. Wang and L. J. Li, Effective doping of single-layer graphene from underlying SiO_2 substrates, *Phys. Rev. B: Condens. Matter Mater. Phys.*, 2009, **79**, 115402.

13 Y.-S. Chen, C.-H. Lee, M.-Y. Hung, H.-A. Pan, J.-C. Chiou and G. S. Huang, DNA sequencing using electrical conductance measurements of a DNA polymerase, *Nat. Nanotechnol.*, 2013, **8**, 452–458.

14 B. M. Venkatesan and R. Bashir, Nanopore sensors for nucleic acid analysis, *Nat. Nanotechnol.*, 2011, **6**, 615–624.

15 J. Kong, N. R. Franklin, C. Zhou, M. G. Chapline, S. Peng, K. Cho, *et al.*, Nanotube molecular wires as chemical sensors, *Science*, 2000, **287**, 622.

16 P. G. Collins, K. Bradley, M. Ishigami and A. Zettl, Extreme oxygen sensitivity of electronic properties of carbon nanotubes, *Science*, 2000, **287**, 1801.

17 E. Snow, F. Perkins, E. Houser, S. Badescu and T. Reinecke, Chemical detection with a single-walled carbon nanotube capacitor, *Science*, 2005, **307**, 1942.

18 Y. B. Shi, J. J. Xiang, Q. H. Feng, Z. P. Hu, H. Q. Zhang and J. Y. Guo, Binary channel SAW mustard gas sensor based on PdPc(0.3)PANI(0.7) hybrid sensitive film, in *4th International Symposium on Instrumentation Science and Technology*, ed. J. Tan, 2006, vol. 48, pp. 292–297.

19 T. Wehling, K. Novoselov, S. Morozov, E. Vdovin, M. Katsnelson, A. Geim, *et al.*, Molecular doping of graphene, *Nano Lett.*, 2008, **8**, 173–177.

20 X. Dong, D. Fu, W. Fang, Y. Shi, P. Chen and L. J. Li, Doping Single-Layer Graphene with Aromatic Molecules, *Small*, 2009, **5**, 1422–1426.

21 N. Mohanty and V. Berry, Graphene-Based Single-Bacterium Resolution Biodevice and DNA Transistor: Interfacing Graphene Derivatives with Nanoscale and Microscale Biocomponents, *Nano Lett.*, 2008, **8**, 4469–4476.

22 M. Zheng, A. Jagota, E. D. Semke, B. A. Diner, R. S. McLean, S. R. Lustig, *et al.*, DNA-assisted dispersion and separation of carbon nanotubes, *Nat. Mater.*, 2003, **2**, 338–342.

23 C. Mastrangelo, DNA analysis systems on a chip, *Adv. Sci. Technol.*, 1999, **26**, 465–476.

24 T. G. Drummond, M. G. Hill and J. K. Barton, Electrochemical DNA sensors, *Nat. Biotechnol.*, 2003, **21**, 1192–1199.

25 E. R. Mardis, Next-generation DNA sequencing methods, *Annu. Rev. Genomics Hum. Genet.*, 2008, **9**, 387–402.

26 M. L. Metzker, Sequencing technologies—the next generation, *Nat. Rev. Genet.*, 2009, **11**, 31–46.

27 Y. Chen, J. Lu and Z. X. Gao, Structural and electronic study of nanoscrolls rolled up by a single graphene sheet, *J. Phys. Chem. C*, 2007, **111**, 1625–1630.

28 A. K. Schaper, H. Q. Hou, M. S. Wang, Y. Bando and D. Golberg, Observations of the electrical behaviour of catalytically grown scrolled graphene, *Carbon*, 2011, **49**, 1821–1828.

29 T. S. Li, M. F. Lin and J. Y. Wu, The effect of a transverse electric field on the electronic properties of an armchair carbon nanoscroll, *Philos. Mag.*, 2011, **91**, 1557–1567.

30 M.-S. Hu, C.-C. Kuo, C.-T. Wu, C.-W. Chen, P. K. Ang, K. P. Loh, *et al.*, The production of SIC nanowalls sheathed with a few layers of strained graphene and their use in heterogeneous catalysis and sensing applications, *Carbon*, 2011, **49**, 4911–4919.

31 J. Zheng, H. T. Liu, B. Wu, Y. L. Guo, T. Wu, G. Yu, *et al.*, Production of High-Quality Carbon Nanoscrolls with Microwave Spark Assistance in Liquid Nitrogen, *Adv. Mater.*, 2011, **23**, 2460–2463.

32 S. F. Braga, V. R. Coluci, S. B. Legoas, R. Giro, D. S. Galvao and R. H. Baughman, Structure and dynamics of carbon nanoscrolls, *Nano Lett.*, 2004, **4**, 881–884.

33 X. H. Shi, N. M. Pugno and H. J. Gao, Tunable Core Size of Carbon Nanoscrolls, *J. Comput. Theor. Nanosci.*, 2010, **7**, 517–521.

34 X. H. Shi, Y. Cheng, N. M. Pugno and H. J. Gao, Tunable Water Channels with Carbon Nanoscrolls, *Small*, 2010, **6**, 739–744.

35 X. A. Peng, J. Zhou, W. C. Wang and D. P. Cao, Computer simulation for storage of methane and capture of carbon dioxide in carbon nanoscrolls by expansion of interlayer spacing, *Carbon*, 2010, **48**, 3760–3768.

36 G. Mpourmpakis, E. Tylianakis and G. E. Froudakis, Carbon nanoscrolls: a promising material for hydrogen storage, *Nano Lett.*, 2007, **7**, 1893–1897.

37 Y. Chen, J. Lu and Z. Gao, Structural and electronic study of nanoscrolls rolled up by a single graphene sheet, *J. Phys. Chem. C*, 2007, **111**, 1625–1630.

38 H. Pan, Y. Feng and J. Lin, *Ab initio* study of electronic and optical properties of multiwall carbon nanotube structures made up of a single rolled-up graphite sheet, *Phys. Rev. B: Condens. Matter Mater. Phys.*, 2005, **72**, 085415.

39 K. S. Novoselov, A. K. Geim, S. V. Morozov, D. Jiang, M. I. Katsnelson, I. V. Grigorieva, *et al.*, Two-dimensional gas of massless Dirac fermions in graphene, *Nature*, 2005, **438**, 197–200.

40 L. X. Dong and Q. Chen, Properties, synthesis, and characterization of graphene, *Frontiers of Materials Science in China*, 2010, vol. 4, pp. 45–51.

41 A. K. Schaper, M. S. Wang, Z. Xu, Y. Bando and D. Golberg, Comparative Studies on the Electrical and Mechanical Behavior of Catalytically Grown Multiwalled Carbon Nanotubes and Scrolled Graphene, *Nano Lett.*, 2011, **11**, 3295–3300.

42 Y. Ouyang, Y. Yoon and J. Guo, Scaling behaviors of graphene nanoribbon FETs: A three-dimensional quantum simulation study, *IEEE Trans. Electron Devices*, 2007, **54**, 2223–2231.

43 X. Dong, Y. Shi, W. Huang, P. Chen and L. J. Li, Electrical Detection of DNA Hybridization with Single-Base Specificity Using Transistors Based on CVD-Grown Graphene Sheets, *Adv. Mater.*, 2010, **22**, 1649–1653.

44 I. Heller, S. Chatoor, J. Mannik, M. A. G. Zevenbergen, C. Dekker and S. G. Lemay, Influence of Electrolyte Composition on Liquid-Gated Carbon Nanotube and Graphene Transistors, *J. Am. Chem. Soc.*, 2010, **132**, 17149–17156.

45 Y. Huang, X. Dong, Y. Liu, L.-J. Li and P. Chen, Graphene-based biosensors for detection of bacteria and their metabolic activities, *J. Mater. Chem.*, 2011, **21**, 12358–12362.

46 M. Dankerl, M. V. Hauf, A. Lippert, L. H. Hess, S. Birner, I. D. Sharp, *et al.*, Graphene Solution-Gated Field-Effect Transistor Array for Sensing Applications, *Adv. Funct. Mater.*, 2010, **20**, 3117–3124.

47 A. Star, E. Tu, J. Niemann, J. C. P. Gabriel, C. S. Joiner and C. Valcke, Label-free detection of DNA hybridization using carbon nanotube network field-effect transistors, *Proc. Natl. Acad. Sci. U. S. A.*, 2006, **103**, 921.

48 R. A. MacDonald, B. F. Laurenzi, G. Viswanathan, P. M. Ajayan and J. P. Stegemann, Collagen–carbon nanotube composite materials as scaffolds in tissue engineering, *J. Biomed. Mater. Res., Part A*, 2005, **74**, 489–496.

49 P. Hu, J. Zhang, L. Li, Z. Wang, W. O'Neill and P. Estrela, Carbon Nanostructure-Based Field-Effect Transistors for Label-Free Chemical/Biological Sensors, *Sensors*, 2010, **10**, 5133–5159.

50 J. Liang, D. Akinwande and H. S. P. Wong, Carrier density and quantum capacitance for semiconducting carbon nanotubes, *J. Appl. Phys.*, 2008, **104**, 064515.

51 M. T. Ahmadi, J. F. Webb, N. A. Amin, S. M. Mousavi, H. Sadeghi and M. R. Neilchiyan, *et al.*, Carbon Nanotube Capacitance Model in Degenerate and Nondegenerate Regimes, in *Proceedings of the Fourth Global Conference on Power Control and Optimization*, ed. N. W. J. F. V. P. Barsoum, 2011, vol. 1337, pp. 173–176.

52 V. Parkash and A. K. Goel, Quantum Capacitance Extraction for Carbon Nanotube Interconnects, *Nanoscale Res. Lett.*, 2010, **5**, 1424–1430.

53 J. Xia, F. Chen, J. Li and N. Tao, Measurement of the quantum capacitance of graphene, *Nat. Nanotechnol.*, 2009, **4**, 505–509.

54 D. Fu and L. J. Li, Label-free electrical detection of DNA hybridization using carbon nanotubes and graphene, *Nano Rev.*, 2010, **1**, 5354.

55 A. T. Johnson Jr, A. Gelperin and C. Staii, Single walled carbon nanotubes functionally adsorbed to biopolymers for use as chemical sensors, Google Patents, 2011.

56 M. Lundstrom and J. Guo, *Nanoscale transistors: Device physics, modeling and simulation*, Springer, New York, 2006, vol. 233.

57 J. W. Wilder, L. C. Venema, A. G. Rinzler, R. E. Smalley and C. Dekker, Electronic structure of atomically resolved carbon nanotubes, *Nature*, 1998, **391**, 59–62.

58 E. T. Model, 3 Carbon Nanotube Field, *Adv. Nanoelectron.*, 2012, **4**, 99.

59 M. T. Ahmadi, Z. Johari, N. A. Amin, S. M. Mousavi and R. Ismail, Carbon nanotube conductance model in parabolic band structure, in *2010 IEEE International Conference on Semiconductor Electronics (ICSE)*, 2010, 256–259.

60 M. T. Ahmadi, Z. Johari, N. A. Amin, A. H. Fallahpour and R. Ismail, Graphene nanoribbon conductance model in parabolic band structure, *J. Nanomater.*, 2010, **2010**, 753738.

61 B. Polash and H. F. Huq, Analytical Model of Carbon Nanotube Field Effect Transistors for NEMS Applications *2008 51st Midwest Symposium on Circuits and Systems*, 2008, vol. 1 and 2, pp. 61–64.

62 M. T. Ahmadi, M. A. Riyadi, I. Saad and R. Ismail, Numerical Study of Fermi energy For P-Type Silicon Nanowire, *Nanosci. Nanotechnol.*, 2009, **1136**, 98–102.

63 J. Karamdel, M. T. Ahmadi, B. Y. Majlis, C. F. Dee and R. Ismail, Formulation and Simulation for Electrical Properties of a (5, 3) Single Wall Carbon Nanotube, *ICSE: 2008 IEEE International Conference on Semiconductor Electronics, Proceedings*, 2008, pp. 545–548.

64 N. Peres, A. H. C. Neto and F. Guinea, Conductance quantization in mesoscopic graphene, *Phys. Rev. B: Condens. Matter Mater. Phys.*, 2006, **73**, 195411.

65 R. B. Dingle and R. Dingle, *Asymptotic expansions: their derivation and interpretation*, Academic Press London, 1973.

66 J. Zaharah, A. Mohammad Taghi, C. Desmond Chang Yih, A. N. Aziziah and I. Razali, Modelling of Graphene Nanoribbon Fermi Energy, *J. Nanomater.*, 2010, **2010**, 909347.

67 D. Gunlycke, D. Areshkin and C. White, Semiconducting graphene nanostrips with edge disorder, *Appl. Phys. Lett.*, 2007, **90**, 142104.

68 H. Ismaili, D. Geng, A. X. Sun, T. T. Kantzas and M. S. Workentin, Light-Activated Covalent Formation of Gold Nanoparticle Graphene and Gold Nanoparticle–Glass Composites, *Langmuir*, 2011, **27**, 13261–13268.

69 M. Tsutsui, Y.-k. Taninouchi, S. Kurokawa and A. Sakai, Electrical breakdown of short multiwalled carbon nanotubes, *J. Appl. Phys.*, 2006, **100**, 094302.

70 M. Anantram, Current-carrying capacity of carbon nanotubes, *Phys. Rev. B: Condens. Matter Mater. Phys.*, 2000, **62**, R4837.

71 A. Svizhenko and M. Anantram, Effect of scattering and contacts on current and electrostatics in carbon nanotubes, *Phys. Rev. B: Condens. Matter Mater. Phys.*, 2005, **72**, 085430.

72 B. Bourlon, D. Glattli, B. Plaçais, J.-M. Berroir, L. Forró and A. Bachtold, Geometrical dependence of high-bias current in multiwalled carbon nanotubes, arXiv preprint cond-mat/0305708, 2003.

73 Q. Chen, S. Wang and L.-M. Peng, Establishing Ohmic contacts for *in situ* current–voltage characteristic measurements on a carbon nanotube inside the scanning electron microscope, *Nanotechnology*, 2006, **17**, 1087.

74 X. Dong, Y. Shi, W. Huang, P. Chen and L.-J. Li, Electrical Detection of DNA Hybridization with Single-Base Specificity Using Transistors Based on CVD-Grown Graphene Sheets, *Adv. Mater.*, 2010, **22**, 1649–1653.

